technology · applications · instrumentation
tai corporation

(NASA-CR-161425) ERROR BUDGET ANALYSIS FOR ADVANCED X-RAY ASTROPHYSICS FACILITY (AXAF) Final Report, Sep. 1979 - Mar. 1980 (TAI Corp., Huntsville, Ala.) 40 p HC A03/MF A01 CSCL 03A G3/89

N80-22149

Unclas
46877

ERROR BUDGET ANALYSIS FOR ADVANCED X-RAY ASTROPHYSICS FACILITY (AXAF)

FINAL REPORT

By

Dietrich Korsch
TAI CORPORATION
12010 S.Memorial Pkwy.
Huntsville,Al. 35803

Prepared for

NATIONAL AERONAUTICS AND SPACE ADMINISTRATION
MARSHALL SPACE FLIGHT CENTER,ALABAMA

Contract NA8-33516

March 1980

TABLE OF CONTENTS

1. SUMMARY

This report summerizes the results of the analytical work that was done on the AXAF telescope during the period from September 1979 to March 1980. Included are the results of a performance evaluation in the presence of aligment errors and surface defects, a sensitivity analysis of every individual subsystem, and a diffraction analysis of the telescope assembly.

2. AXAF PERFORMANCE ANALYSIS

The performance evaluation of the AXAF telescope system in the presence of aligment and figure errors as presented in the final report, NAS8-33158, entitled "AXAF OPTICAL TECHNOLOGY ANALYSIS" has been continued.

In addition to aligment and figure errors, we now change the surface reflectivities, which were previously assumed to be one, to the corresponding calculated values for certain coa= ting materials and wavelengths. It is assumed that the three outer systems are nickel-coated and the three inner systems are gold-coated. The reflectivities and effective areas (geo-- metric area x reflectivity squared) for different wavelengths.

AU

WAVELENGTH (A): 2

SYSTEM	GRAZ ANG (RAD)	REFLECTIVITY	EFF AREA (SQ IN)
1	0.015	0.079709382	0.457331092
2	0.013517768	0.174547064	1.812462648
3	0.012068919	0.413908125	8.274752919
4	0.010653141	0.605363702	13.67648170
5	9.27015E-03	0.705747147	13.87150113
6	7.91969E-03	0.771243543	11.79521324

WAVELENGTH (A): 10.44

SYSTEM	GRAZ ANG (RAD)	REFLECTIVITY	EFF AREA (SQ IN)
1	0.015	0.793923223	45.37000772
2	0.013517768	0.813529435	39.37227508
3	0.012068919	0.832741237	33.4940198
4	0.010653141	0.851597144	27.06512438
5	9.27015E-03	0.870130579	21.0859932
6	7.91969E-03	0.888370439	15.64987639

WAVELENGTH (A): 47.68

SYSTEM	GRAZ ANG (RAD)	REFLECTIVITY	EFF AREA (SQ IN)
1	0.015	0.886549686	56.57414549
2	0.013517768	0.897215487	47.88919008
3	0.012068919	0.907748657	39.79956827
4	0.010653141	0.918146716	31.46051338
5	9.27015E-03	0.928406950	24.0050141
6	7.91969E-03	0.938526412	17.4668951

WAVELENGTH (A): 183.32

SYSTEM	GRAZ ANG (RAD)	REFLECTIVITY	EFF AREA (SQ IN)
1	0.015	0.980027911	69.13352978
2	0.013517768	0.981986039	57.36600361
3	0.012068919	0.983903093	46.75755385
4	0.010653141	0.985779363	36.26611874
5	9.27015E-03	0.987615096	27.16443264
6	7.91969E-03	0.989410501	19.41224414

NI

WAVELENGTH (A): 2

SYSTEM	GRAZ ANG (RAD)	REFLECTIVITY	EFF AREA (SQ IN)
1	0.015	0.013589083	0.013292056
2	0.013517768	0.023429777	0.032657301
3	0.012068919	0.045028034	0.097929402
4	0.010653141	0.105957417	0.418990677
5	9.27015E-03	0.498928581	6.932692948
6	7.91969E-03	0.890820653	15.73632326

WAVELENGTH (A): 10.44

SYSTEM	GRAZ ANG (RAD)	REFLECTIVITY	EFF AREA (SQ IN)
1	0.015	0.716278549	36.92969598
2	0.013517768	0.742726777	32.81724593
3	0.012068919	0.768706453	28.54093419
4	0.010653141	0.794281523	23.54455868
5	9.27015E-03	0.819508196	18.70388408
6	7.91969E-03	0.844435784	14.14021368

WAVELENGTH (A): 47.68

SYSTEM	GRAZ ANG (RAD)	REFLECTIVITY	EFF AREA (SQ IN)
1	0.015	0.924563678	61.52979925
2	0.013517768	0.931795926	51.65181462
3	0.012068919	0.938908164	42.57879448
4	0.010653141	0.945900388	33.39123196
5	9.27015E-03	0.952772399	25.28154054
6	7.91969E-03	0.959523798	18.25720176

WAVELENGTH (A): 103.32

SYSTEM	GRAZ ANG (RAD)	REFLECTIVITY	EFF AREA (SQ IN)
1	0.015	0.919869111	60.90653782
2	0.013517768	0.927499766	51.17661847
3	0.012068919	0.935017471	42.27664549
4	0.010653141	0.942420515	33.14599783
5	9.27015E-03	0.949707097	25.11912843
6	7.91969E-03	0.956875325	18.15655400

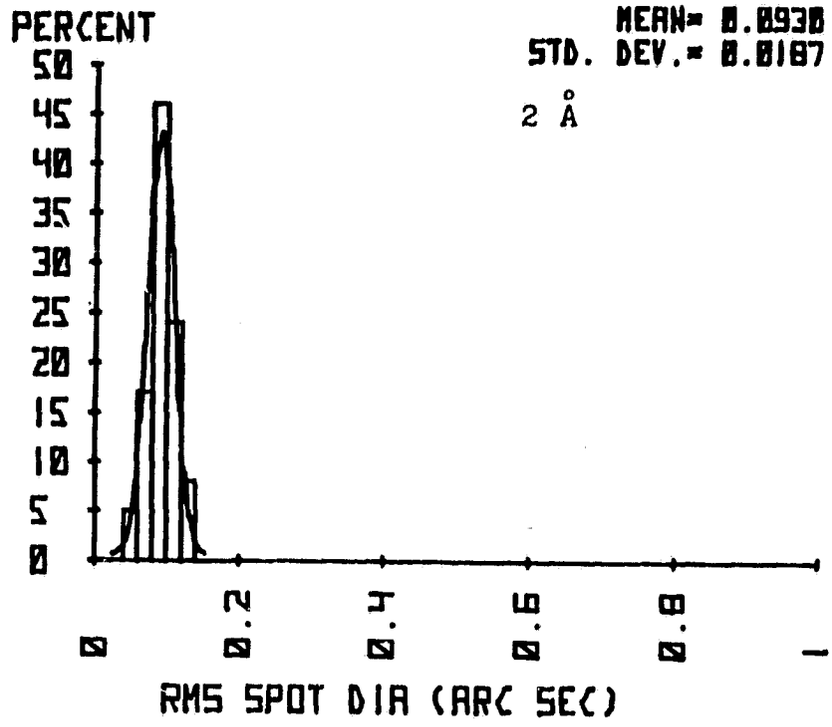

Fig. 1:

Performance in the presence of linear misalignments only; -10^{-4} in. $\leq$ LM $\leq + 10^{-4}$ in.

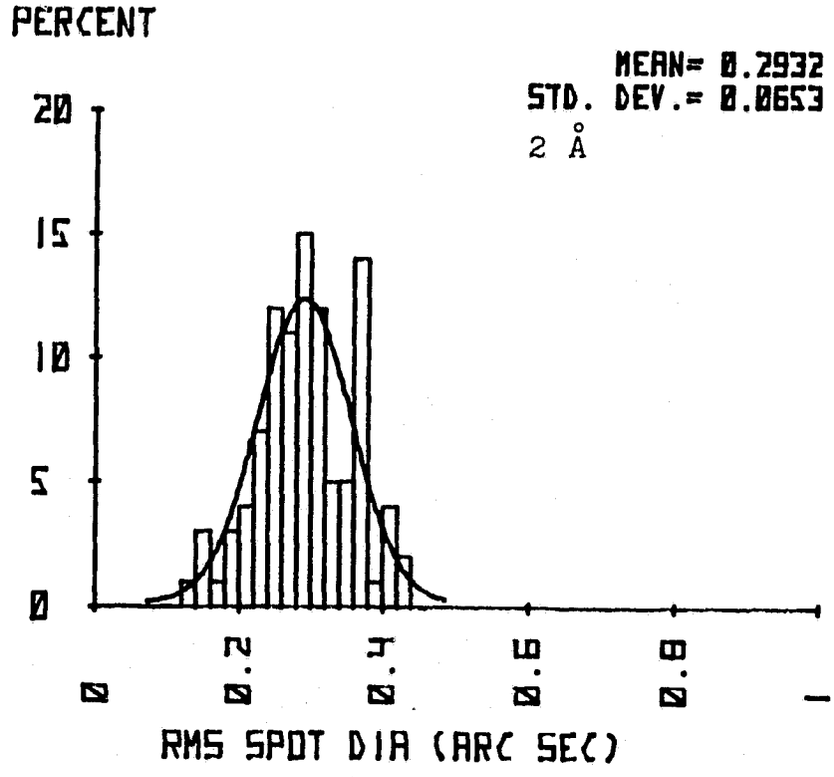

Fig. 2:

Performance in the presence of angular misalignments only; $-5 \cdot 10^{-7}$ rad $\leq$ AM $\leq +5 \cdot 10^{-7}$ rad.

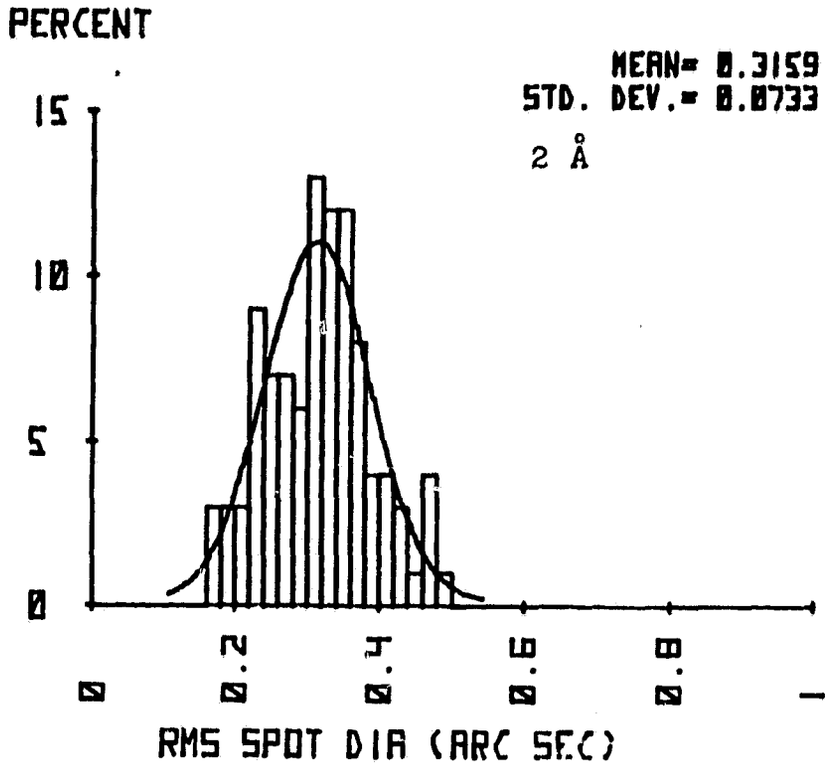

Fig. 3:
Performance in the presence of linear and angular misalignments; -10^{-4} in. $\leq$ LM $\leq +10^{-4}$ in., $-5 \cdot 10^{-7}$ rad $\leq$ AM $\leq +5 \cdot 10^{-7}$ rad.

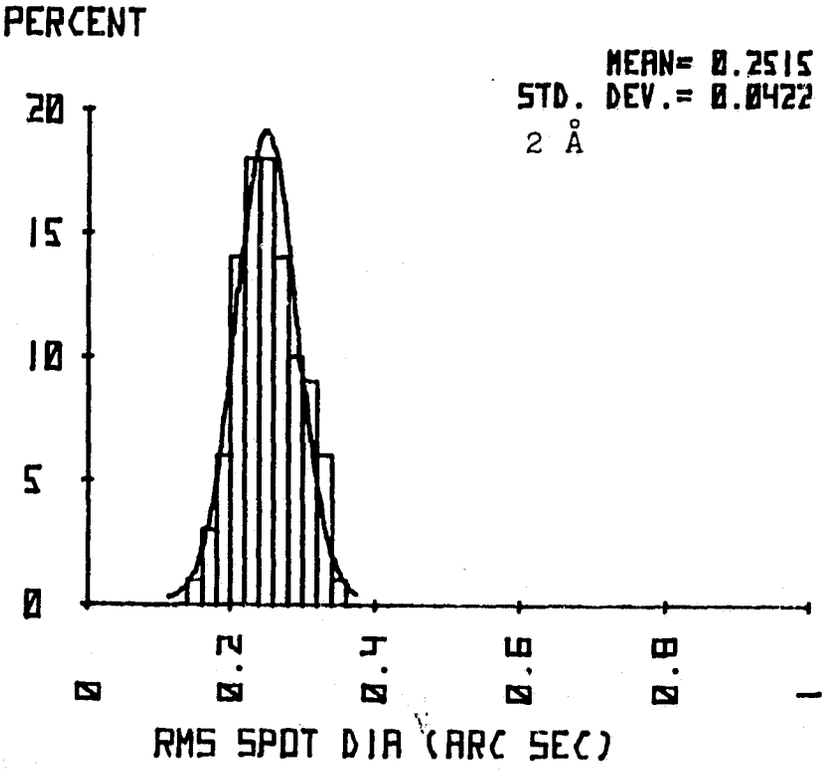

Fig. 4:
Performance in the presence of figure errors only; FE = $5 \cdot 10^{-7}$ rad.

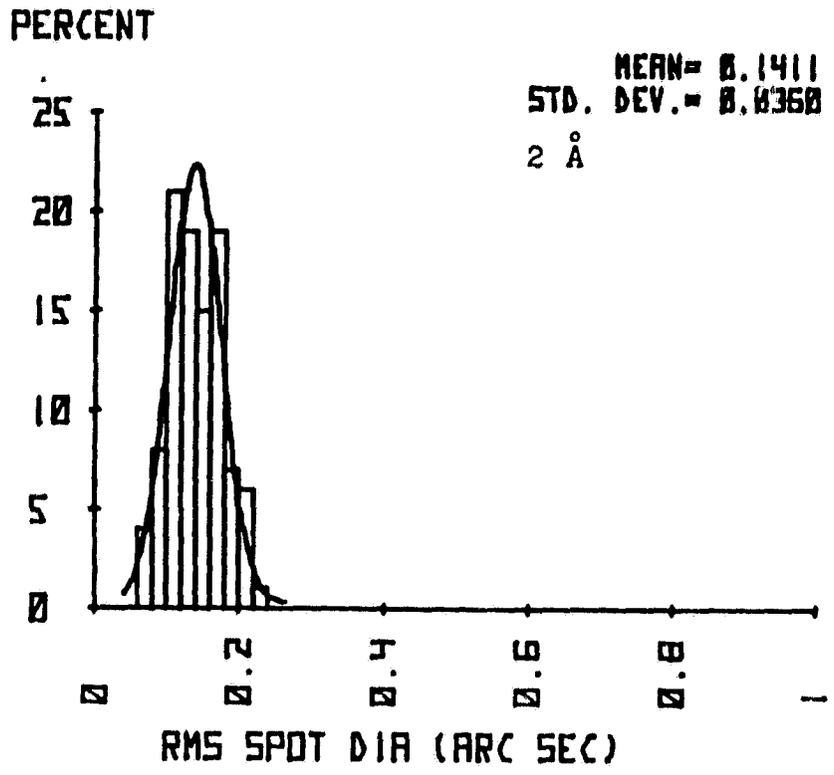

Fig. 5:
Performance in the presence of figure errors only; $-5 \cdot 10^{-7}$ rad $\leq$ FE $\leq +5 \cdot 10^{-7}$ rad.

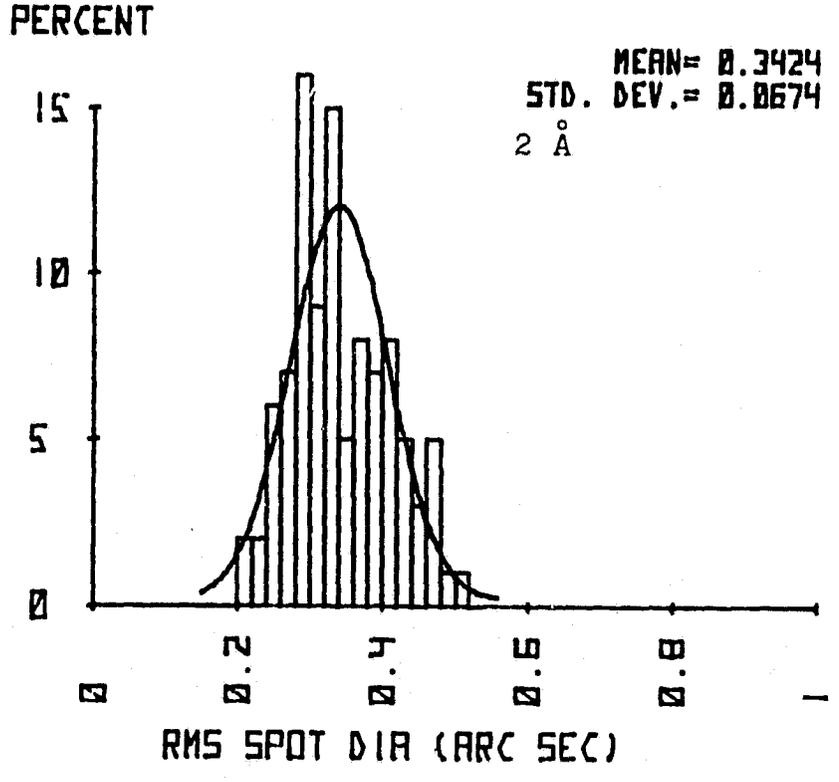

Fig. 6:
Performance in the presence of alignment and figure errors; -10^{-4} in. $\leq$ LM $\leq +10^{-4}$ in., $-5 \cdot 10^{-7}$ rad $\leq$ AM $\leq +5 \cdot 10^{-4}$ rad, $-5 \cdot 10^{-7}$ rad $\leq$ FE $\leq +5 \cdot 10^{-7}$rad.

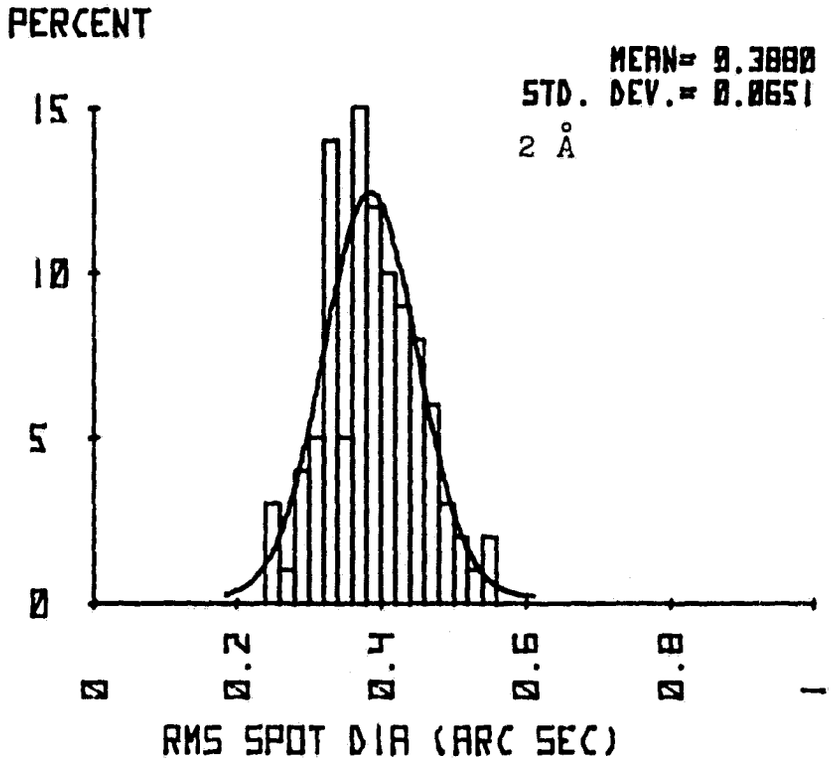

Fig. 7:
Performance in the presence of alignment and figure errors; -10^{-4} in. $\leq$ LM $\leq +10^{-4}$ in., $-5 \cdot 10^{-7}$ rad $\leq$ AM $\leq +5 \cdot 10^{-7}$rad, FE = $5 \cdot 10^{-7}$rad.

Fig. 8;
Performance in the presence of linear misalignments only; -10^{-4} in. $\leq$ LM $\leq + 10^{-4}$ in.

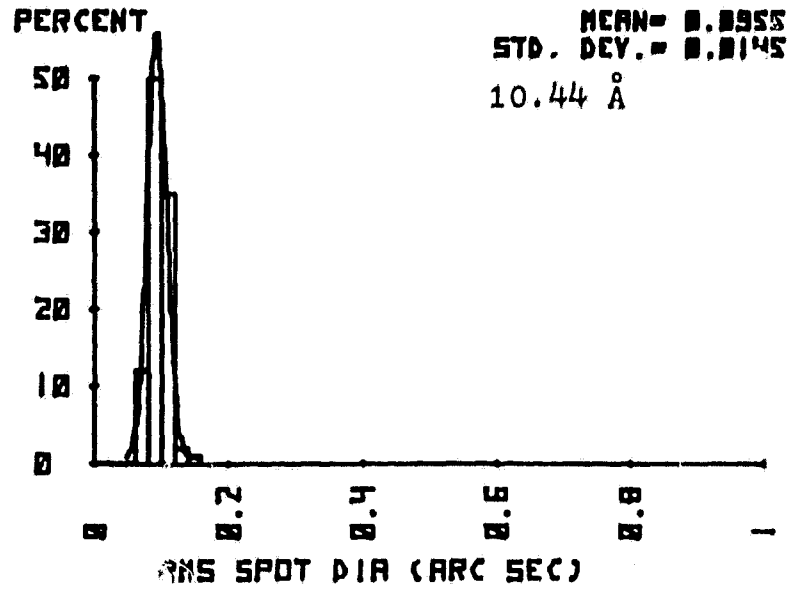

Fig. 9;
Performance in the presence of angular misalignments only; $-5 \cdot 10^{-7}$ rad $\leq$ AM $\leq +5 \cdot 10^{-7}$ rad.

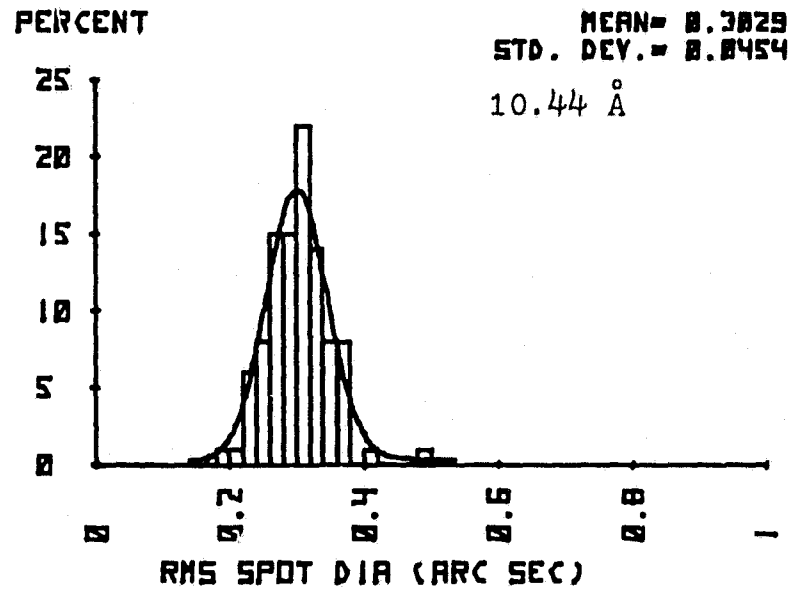

Fig. 10:

Performance in the presence of linear and angular misalignments; -10^{-4} in. $\leq$ LM $\leq +10^{-4}$ in., $-5 \cdot 10^{-7}$ rad $\leq$ AM $\leq +5 \cdot 10^{-7}$ rad.

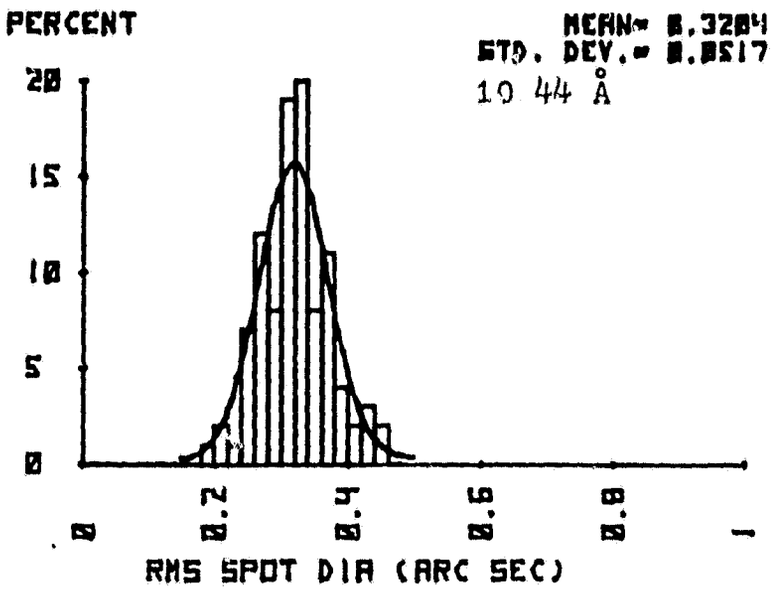

Fig.11:

Performance in the presence of figure errors only; FE = $5 \cdot 10^{-7}$ rad.

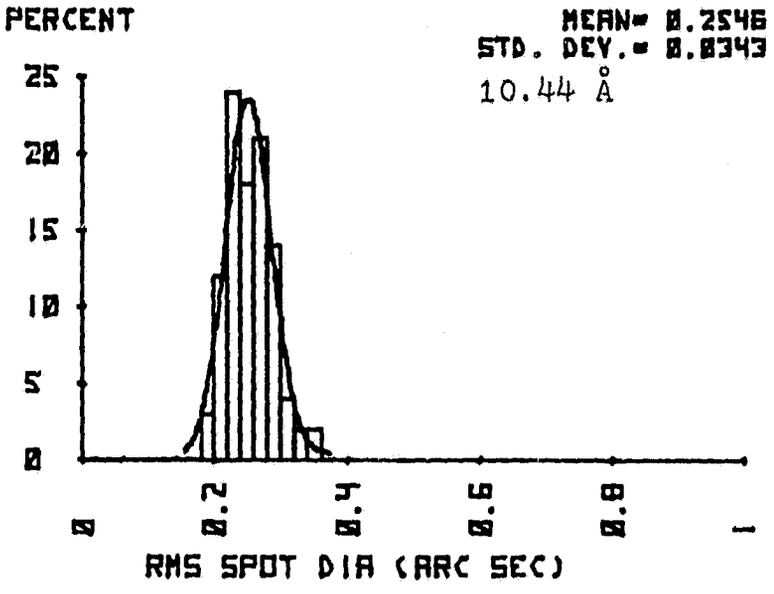

Fig.12:
Performance in the presence of figure errors only;
$-5 \cdot 10^{-7}$ rad $\leq$ FE $\leq +5 \cdot 10^{-7}$ rad.

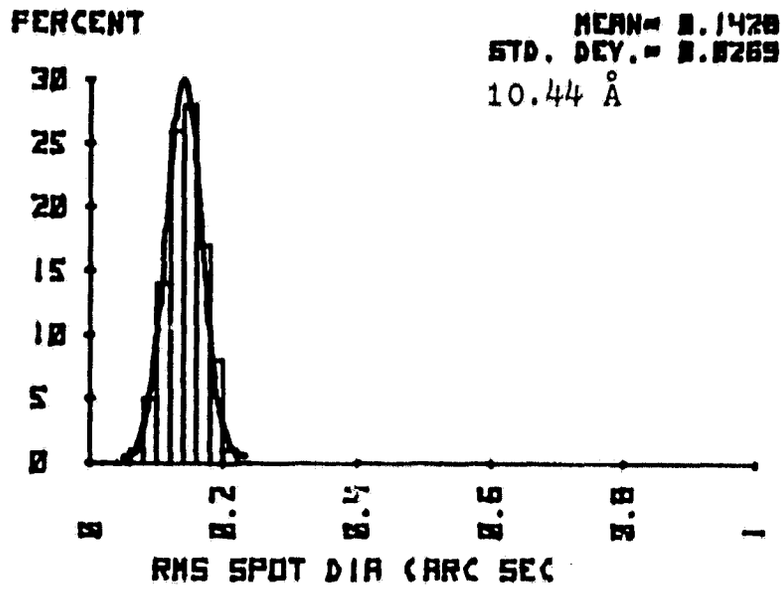

Fig. 13:
Performance in the presence of alignment and figure errors; -10^{-4} in. $\leq$ LM $\leq +10^{-4}$ in., $-5 \cdot 10^{-7}$ rad $\leq$ AM $\leq +5 \cdot 10^{-4}$ rad, $-5 \cdot 10^{-7}$ rad $\leq$ FE $\leq +5 \cdot 10^{-7}$rad.

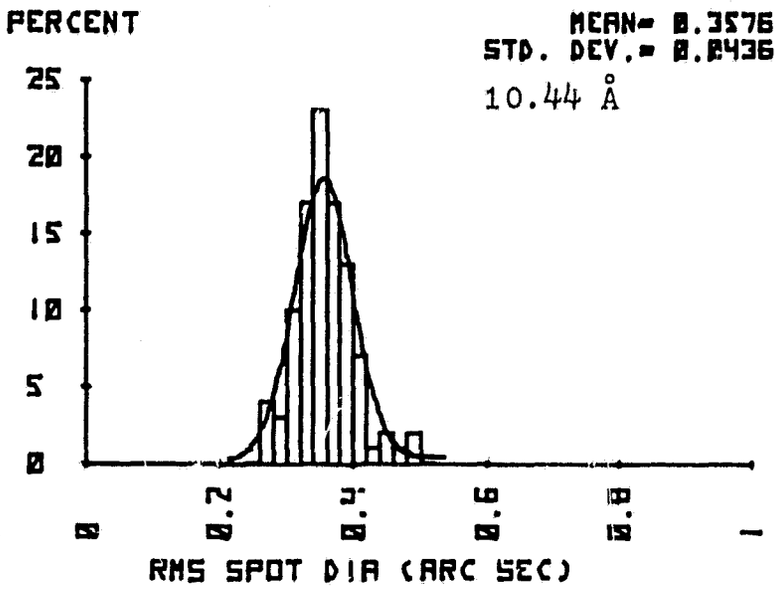

Fig. 14:

Performance in the presence of alignment and figure errors; -10^{-4} in. $\leq$ LM $\leq +10^{-4}$ in., $-5 \cdot 10^{-7}$ rad $\leq$ AM $\leq +5 \cdot 10^{-7}$rad, FE = $5 \cdot 10^{-7}$rad.

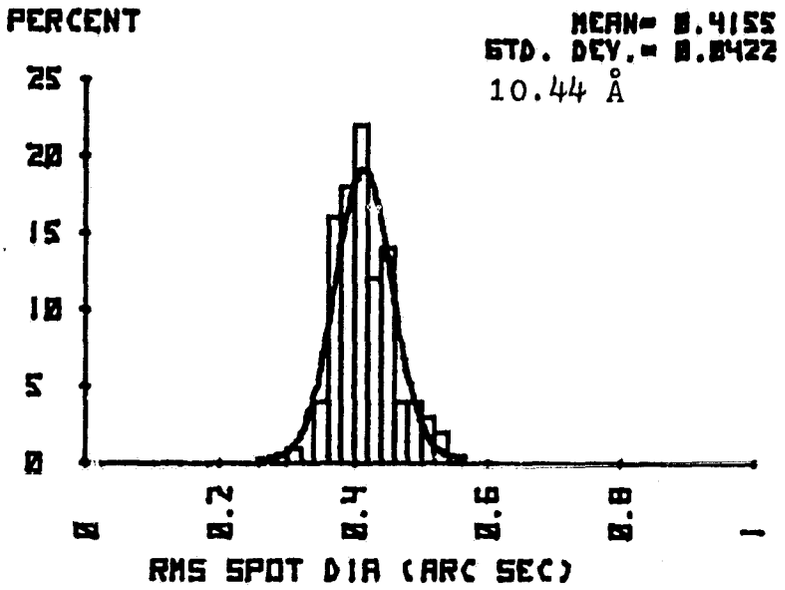

Fig. 15:
Performance in the presence of linear misalignments only; -10^{-4} in. $\leq$ LM $\leq + 10^{-4}$ in.

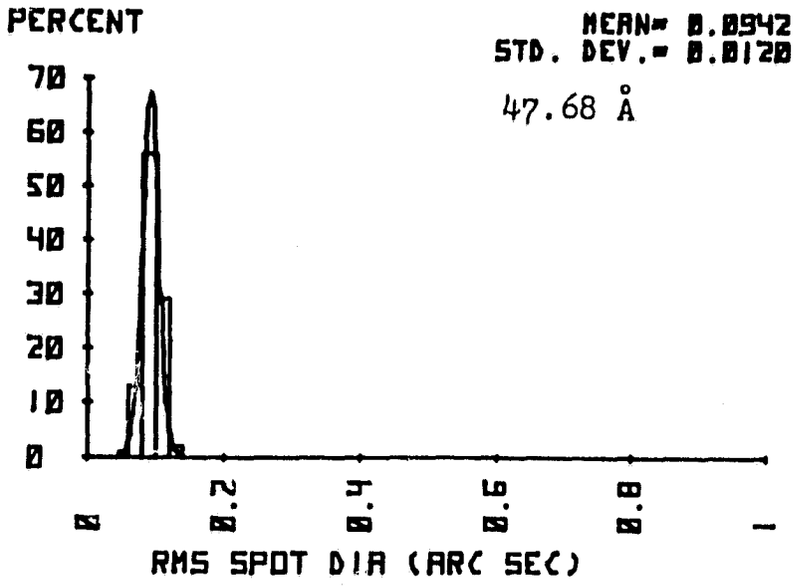

Fig. 16:
Performance in the presence of angular misalignments only; $-5 \cdot 10^{-7}$ rad $\leq$ AM $\leq +5 \cdot 10^{-7}$ rad.

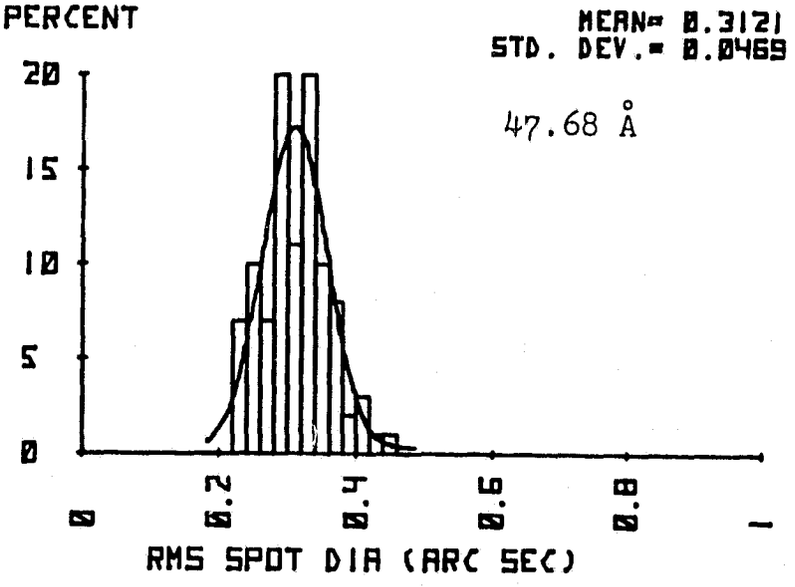

Fig. 17:
Performance in the presence of linear and angular misalignments; -10^{-4} in. $\leq$ LM $\leq +10^{-4}$ in., $-5 \cdot 10^{-7}$ rad $\leq$ AM $\leq +5 \cdot 10^{-7}$ rad.

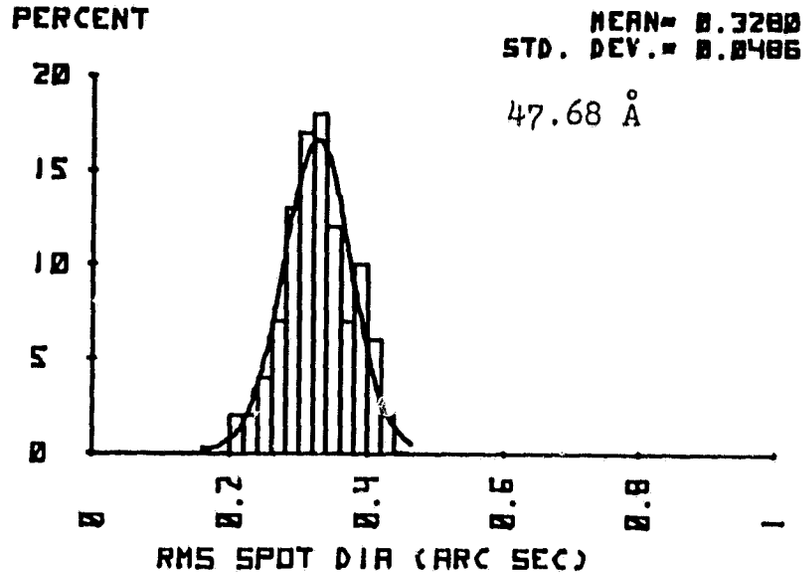

Fig. 18:
Performance in the presence of figure errors only; FE = $5 \cdot 10^{-7}$ rad.

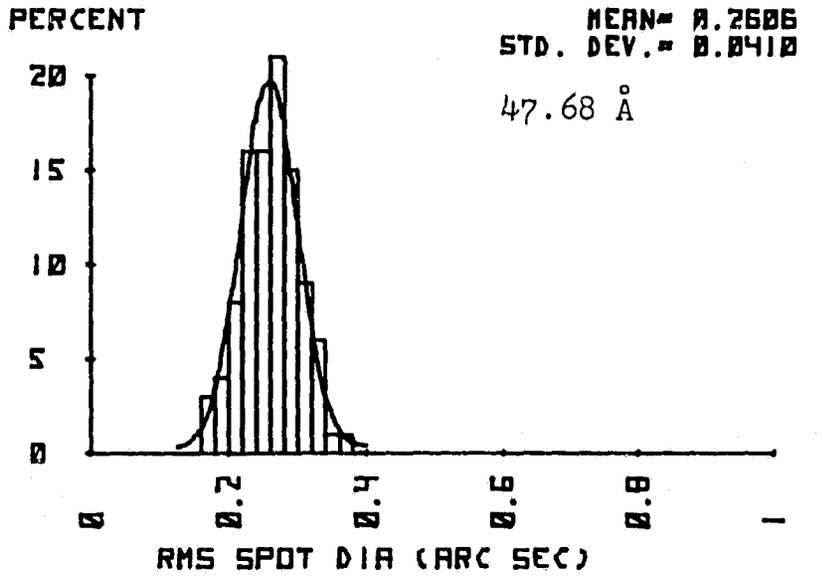

Fig.19:

Performance in the presence of figure errors only;
$-5 \cdot 10^{-7}$ rad $\leq$ FE $\leq +5 \cdot 10^{-7}$ rad.

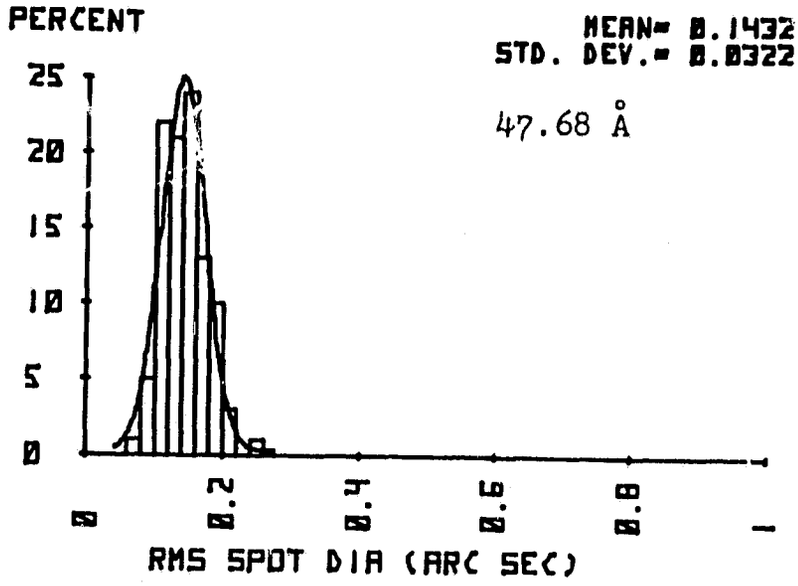

Fig. 20:

Performance in the presence of alignment and figure errors; -10^{-4} in. $\leq$ LM $\leq +10^{-4}$ in., $-5 \cdot 10^{-7}$ rad $\leq$ AM $\leq +5 \cdot 10^{-4}$ rad, $-5 \cdot 10^{-7}$ rad $\leq$ FE $\leq +5 \cdot 10^{-7}$rad.

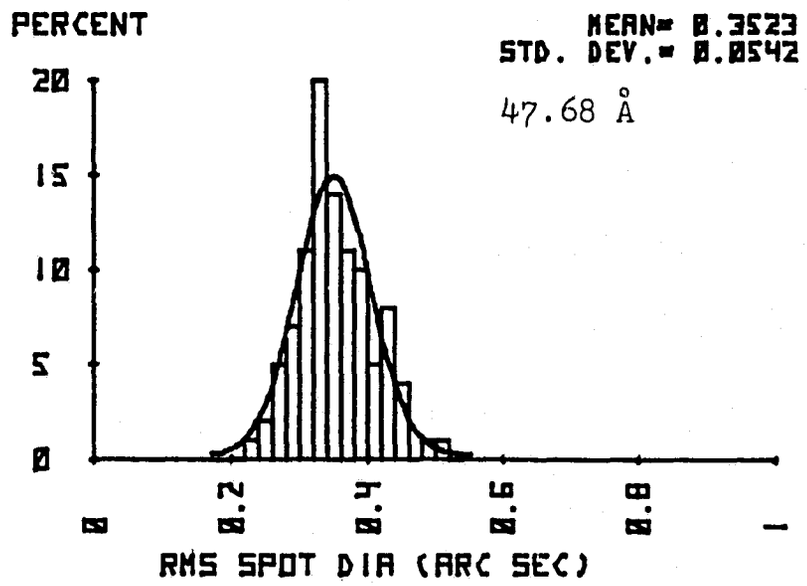

Fig. 21:

Performance in the presence of alignment and figure errors; -10^{-4} in. $\leq$ LM $\leq +10^{-4}$ in., $-5 \cdot 10^{-7}$ rad $\leq$ AM $\leq +5 \cdot 10^{-7}$rad, FE = $5 \cdot 10^{-7}$rad.

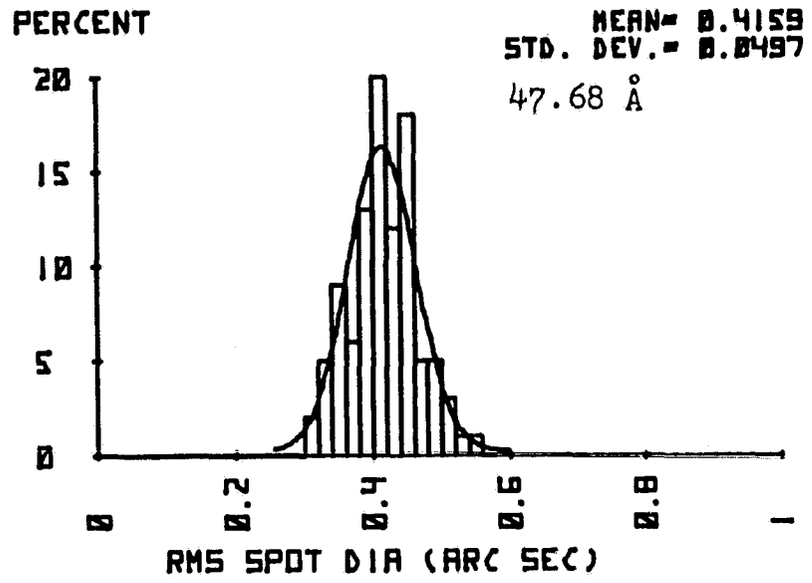

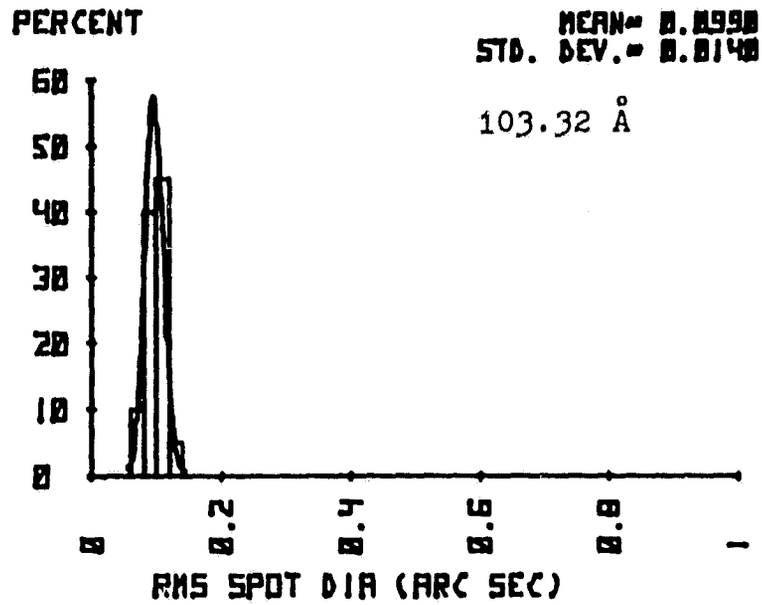

Fig.22:
Performance in the presence of linear misalignments only; -10^{-4} in. $\leq$ LM $\leq + 10^{-4}$ in.

103.32 Å

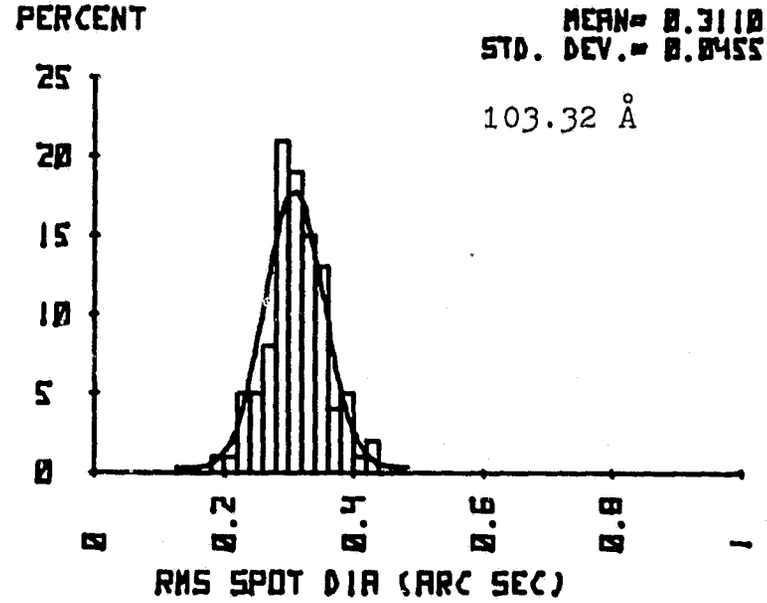

Fig. 23:
Performance in the presence of angular misalignments only; $-5 \cdot 10^{-7}$ rad $\leq$ AM $\leq +5 \cdot 10^{-7}$ rad.

103.32 Å

Fig. 24:
Performance in the presence of linear and angular misalignments; -10^{-4} in. $\leq$ LM $\leq + 10^{-4}$ in., $-5 \cdot 10^{-7}$ rad $\leq$ AM $\leq +5 \cdot 10^{-7}$ rad.

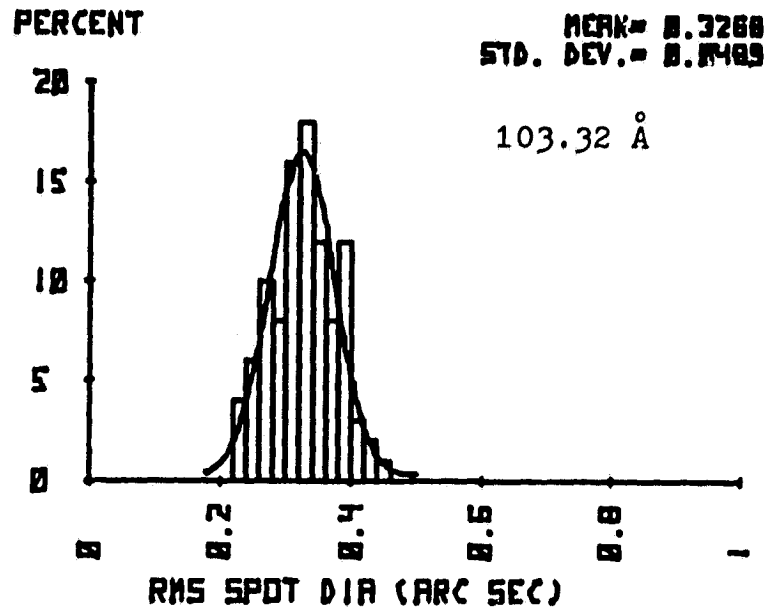

Fig. 25:
Performance in the presence of figure errors only; FE = $5 \cdot 10^{-7}$ rad.

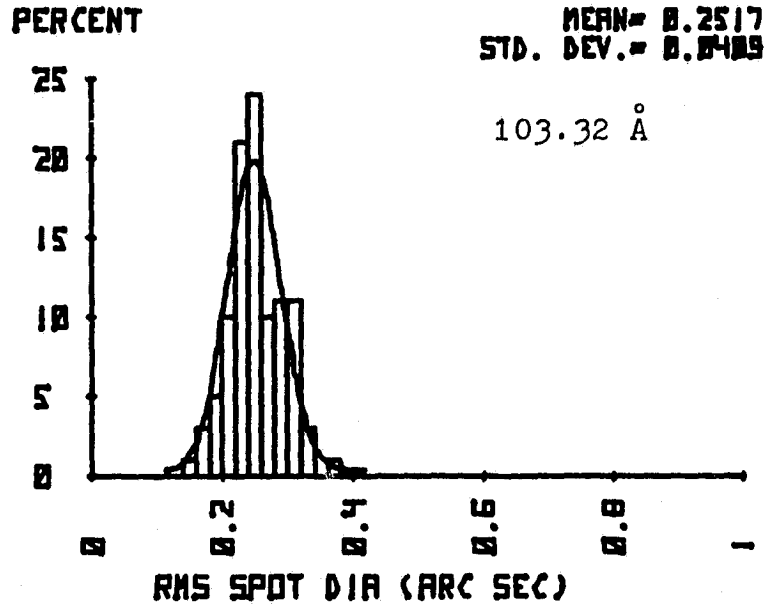

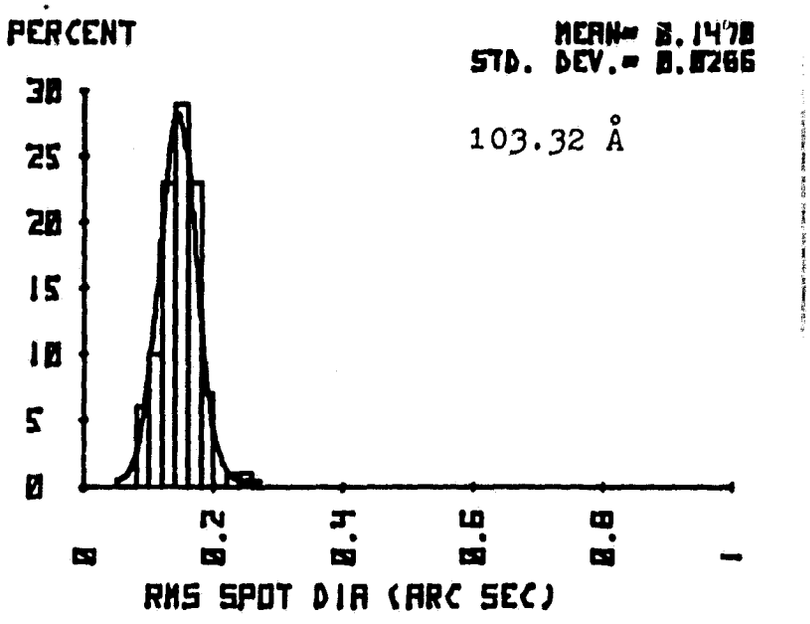

Fig. 26:
Performance in the presence of figure errors only;
$-5 \cdot 10^{-7}$ rad $\leq$ FE $\leq +5 \cdot 10^{-7}$ rad.

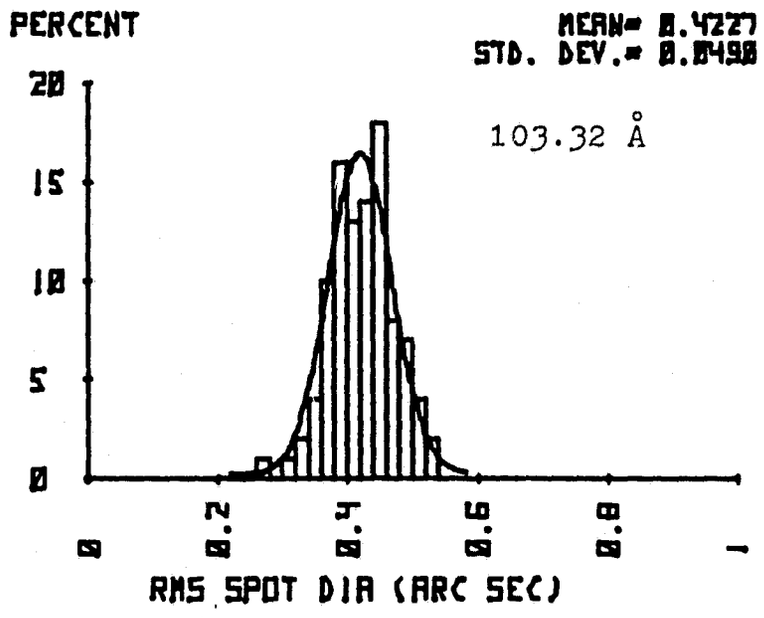

Fig. 27:
Performance in the presence of alignment and figure errors; -10^{-4} in. $\leq$ LM $\leq +10^{-4}$ in., $-5 \cdot 10^{-7}$ rad $\leq$ AM $\leq +5 \cdot 10^{-4}$ rad, $-5 \cdot 10^{-7}$ rad $\leq$ FE $\leq +5 \cdot 10^{-7}$rad.

Fig.28:

Performance in the presence of alignment and figure errors; -10^{-4} in. $\leq$ LM $\leq +10^{-4}$ in., $-5 \cdot 10^{-7}$ rad $\leq$ AM $\leq +5 \cdot 10^{-7}$rad, FE = $5 \cdot 10^{-7}$rad.

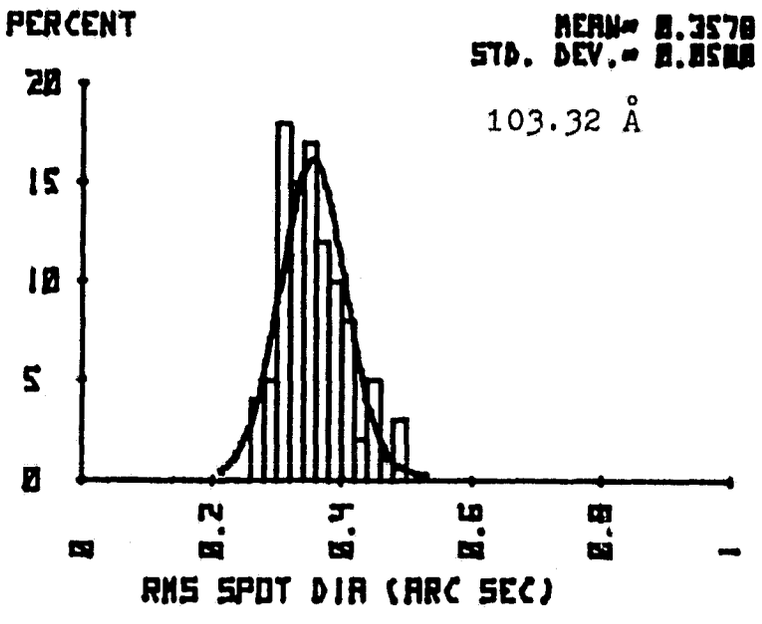

3. MISALIGMENT SENSITIVITIES

The final report entitled "ANALYSIS AND DESIGN OPTIMISATION OF THE 1.2m X-RAY TELESCOPE" (July 78) contains a table with misaligment sensitivities for the individual telescope subsystems. This table includes a column called DESPACE. The text, however, does not explain how these despace sensitivities were generated. There are actually two ways to do this, as shown in Fig.29. One can move the primary (dp) in a system where the secondary and the focal point remain fixed, and one can move the secondary (ds) in a system where the primary and the focal point remain fixed. Each case results in a different effect on the performance. A complete listing of misaligment sensitivities is given in Table 1. The tilt values are for tilts about the center of the secondary. The effects of tilt on the axial spot size growth as the function of the location of the center of rotation on the optical axis is shown in Fig.30. The spot size growth approaches zero as expected at the so-called neutral piont. Fig.31 shows schematically the position of the neutral point with respect to the mirror assembly and its system focal point.

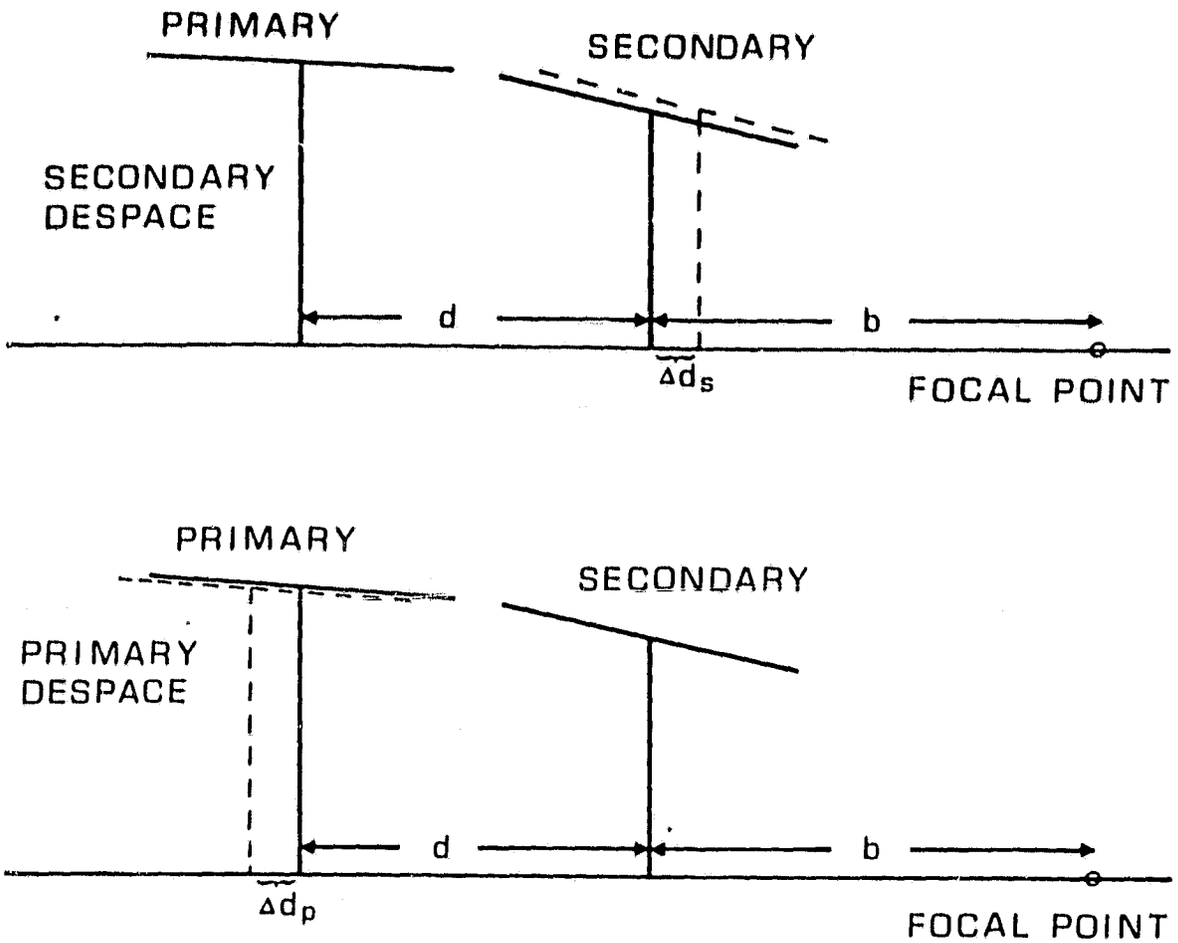

Fig. 29: Primary and Secondary Despace

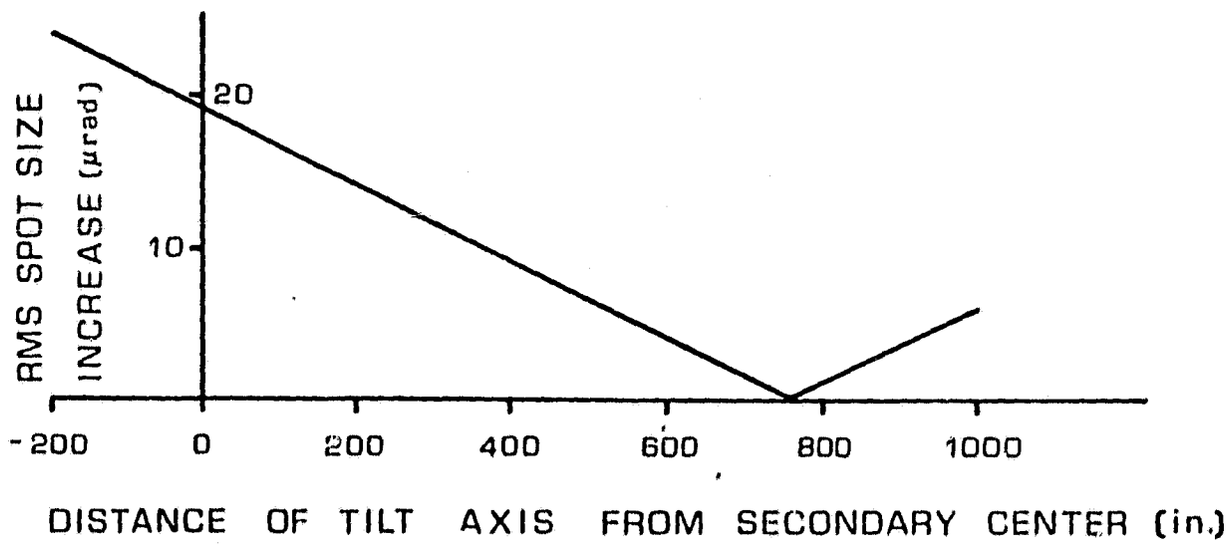

Fig. 30: Growth of the axial spot size due to tilt as a function of location of the center of rotation.

TABLE 1: MISALIGNMENT SENSITIVITIES

SYSTEM NO.	PRIMARY DESPACE	SECONDARY DESPACE	DECENTER	TILT
1	0.0030μrad/μm	0.015μrad/μm	0.1μrad/μm	1.9μrad/μrad
2	0.0027μrad/μm	0.013μrad/μm	0.1μrad/μm	1.9μrad/μrad
3	0.0024μrad/μm	0.012μrad/μm	0.1μrad/μm	1.9μrad/μrad
4	0.0021μrad/μm	0.011μrad/μm	0.1μrad/μm	1.9μrad/μrad
5	0.0018μrad/μm	0.009μrad/μm	0.1μrad/μm	1.9μrad/μrad
6	0.0016μrad/μm	0.008μrad/μm	0.1μrad/μm	1.9μrad/μrad

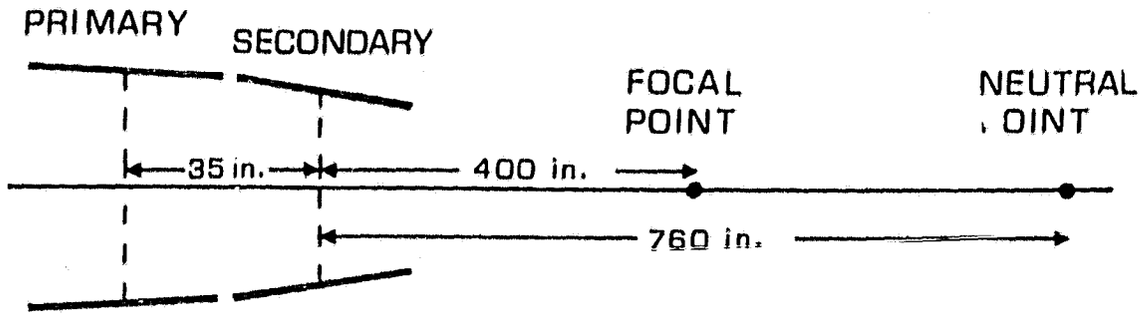

Fig. 31: Location of the neutral point

4. DIFFRACTION ANALYSIS

Diffraction patterns of annular entrance apertures corresponding to the outer element of the AXAF telescope and of the entire composite system for visible and x-ray wavelengths have been calculated and plotted in figs.32 to 43.These analysis reflect the performance at the gaussian focal point for ideal systems.

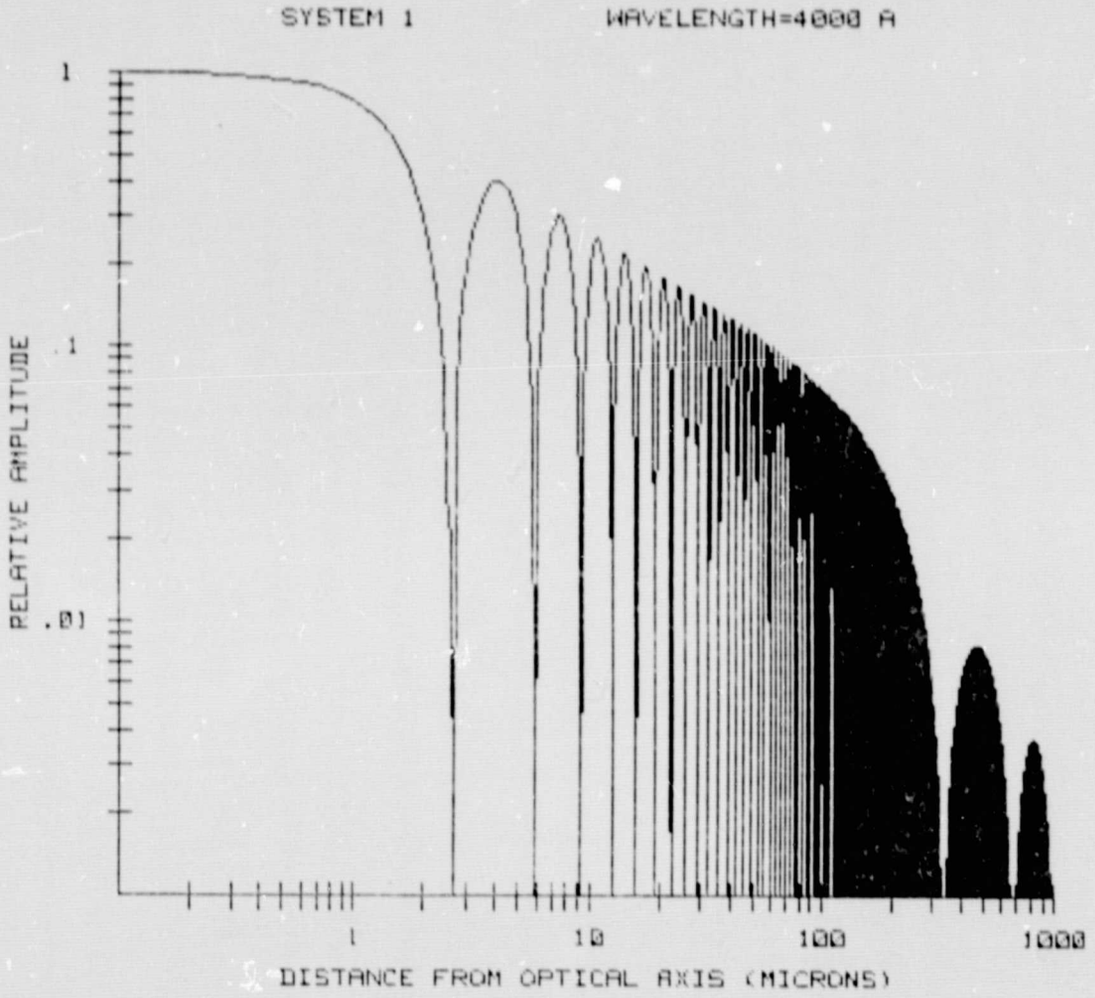

Fig. 32: Diffraction analysis of outer system

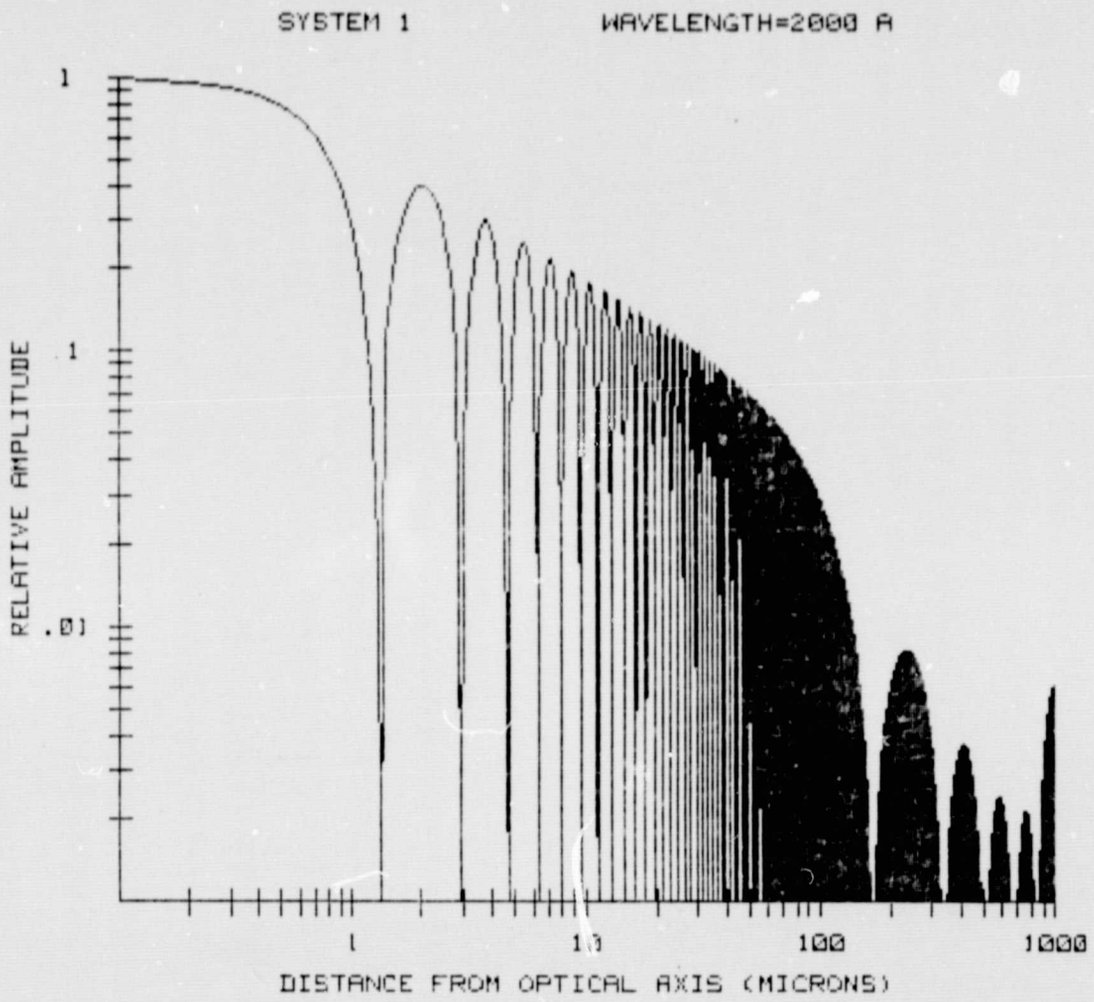

Fig. 33: Diffraction analysis of outer system

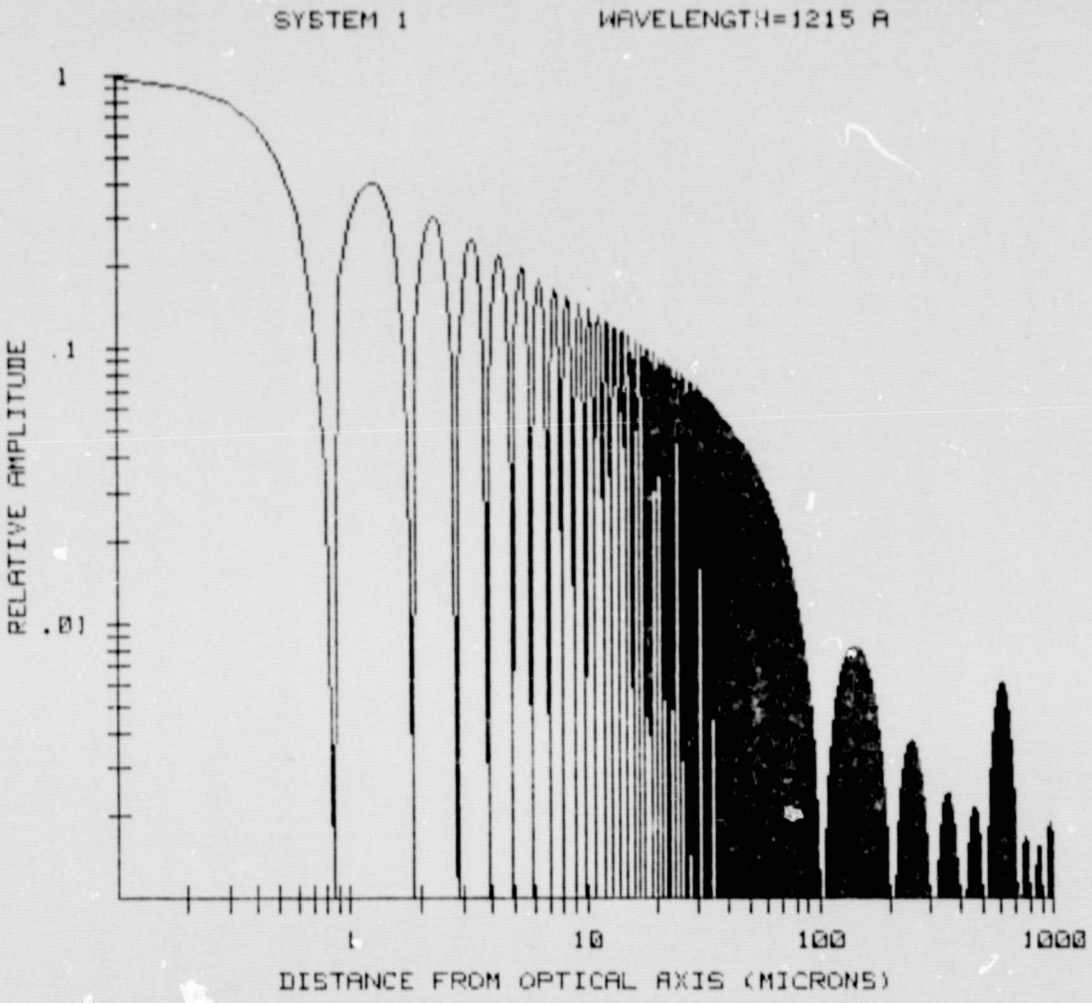

Fig. 34: Diffraction analysis of outer system

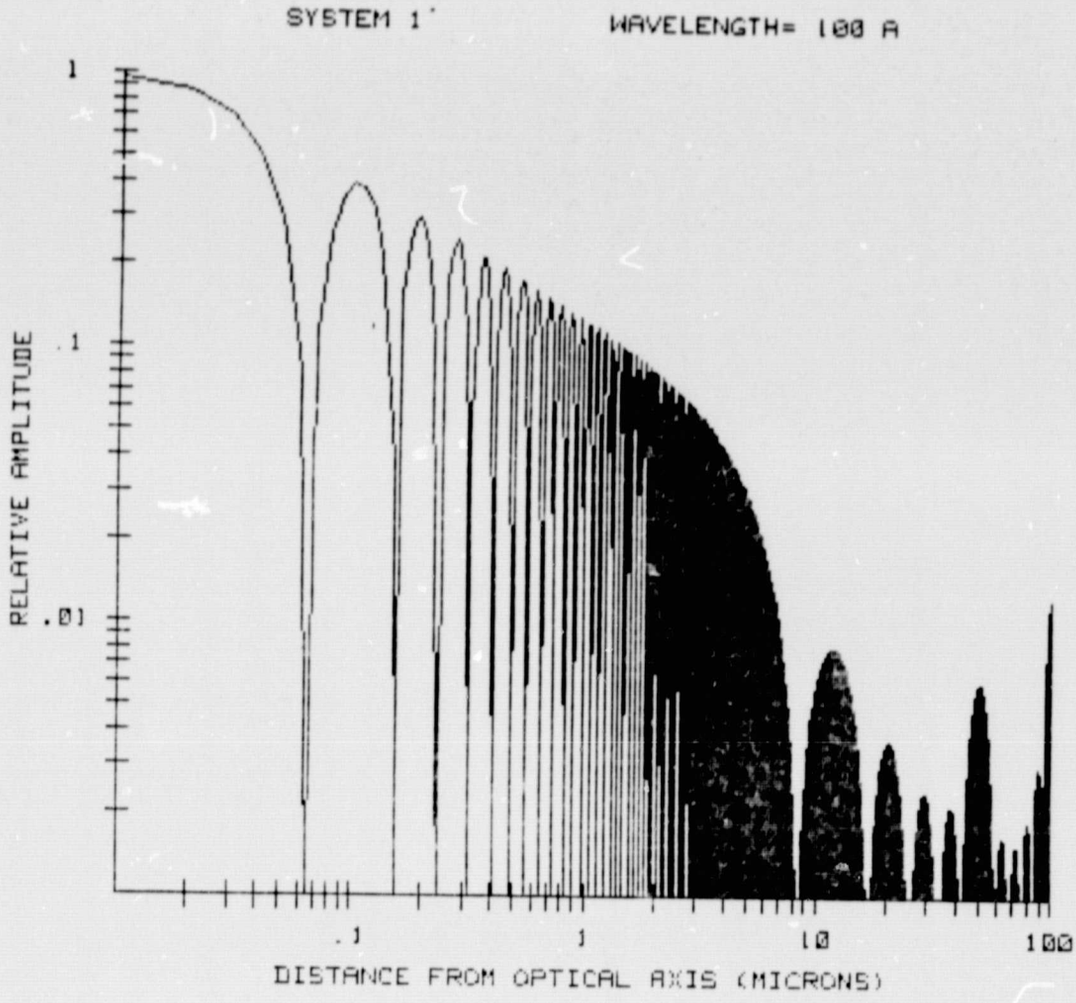

Fig. 35: Diffraction analysis of outer system

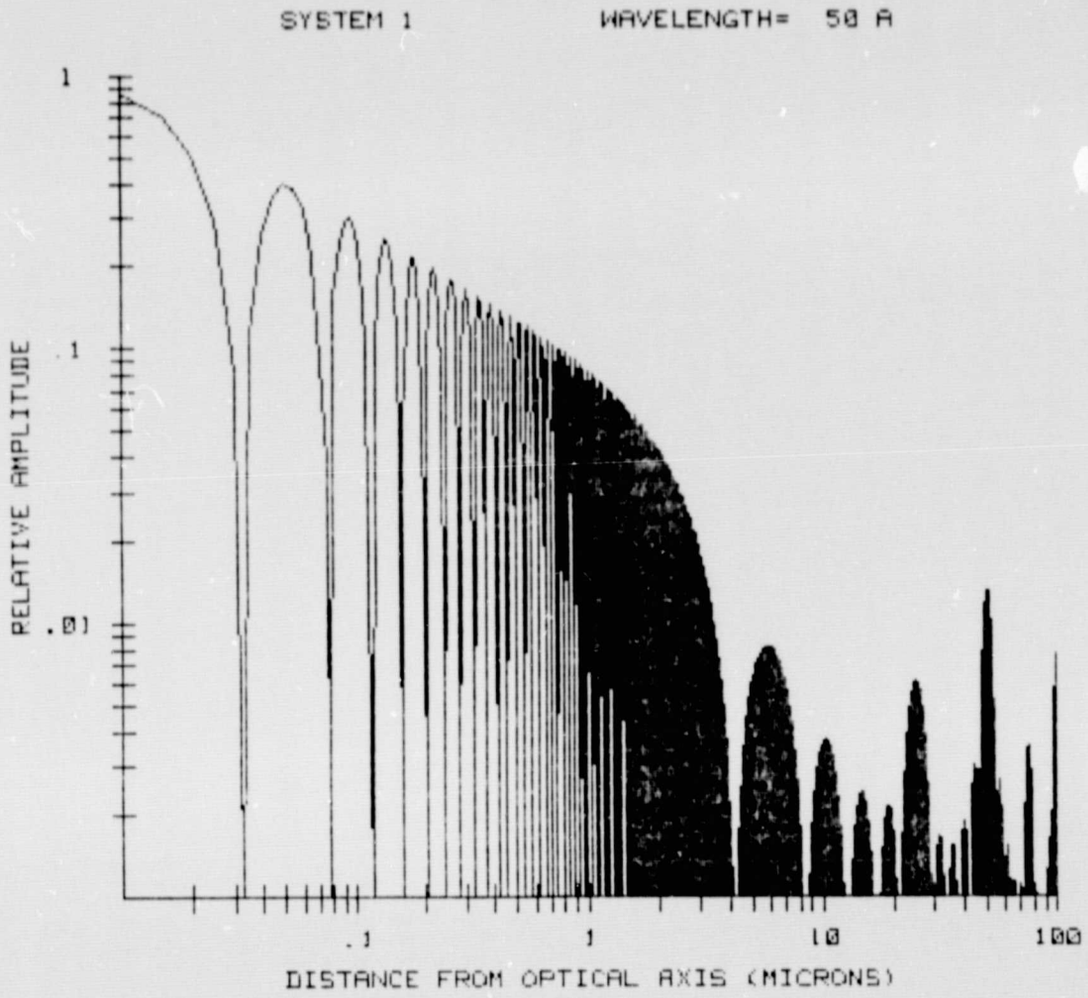

Fig. 36: Diffraction analysis of outer system

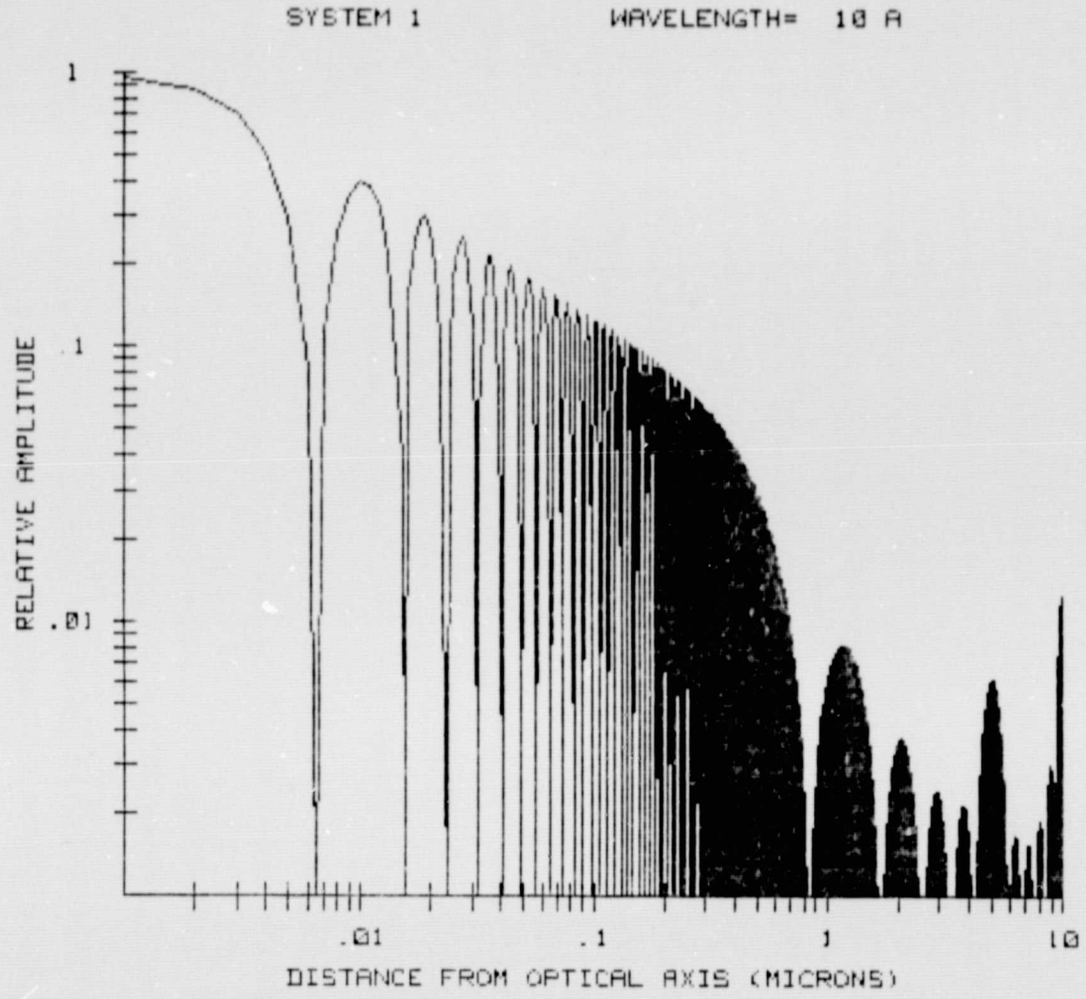

Fig. 37: Diffraction analysis of outer system

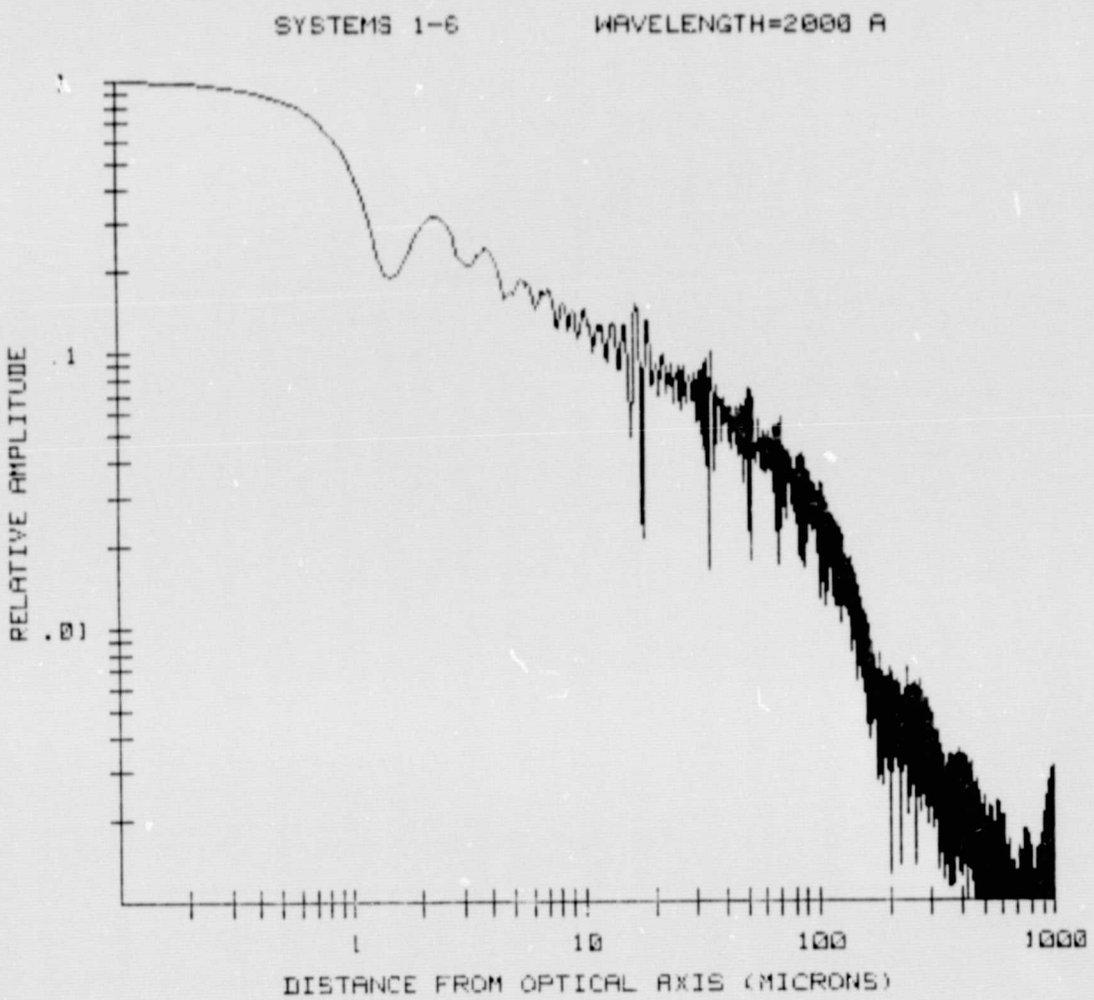

Fig. 39: Diffraction analysis of composite system

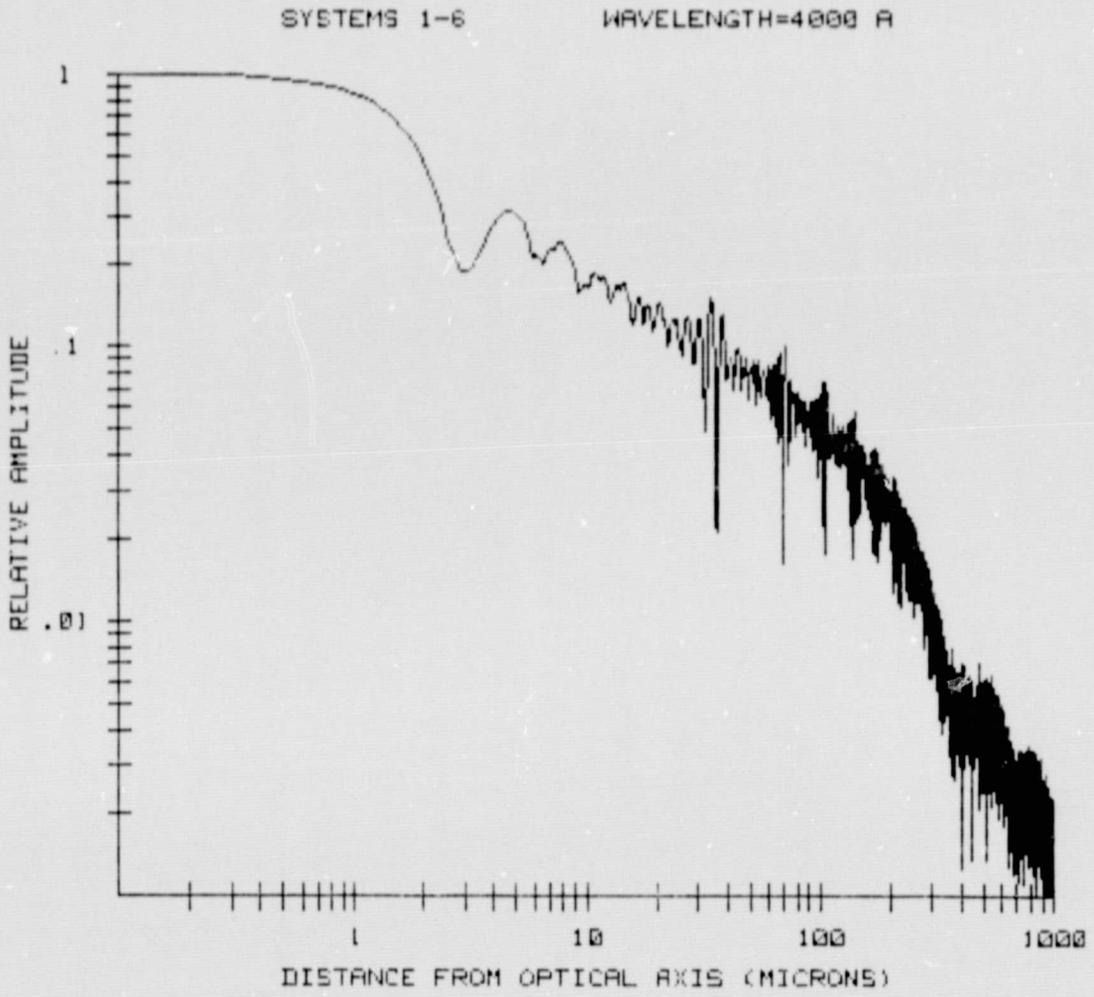

Fig. 38: Diffraction analysis of composite system

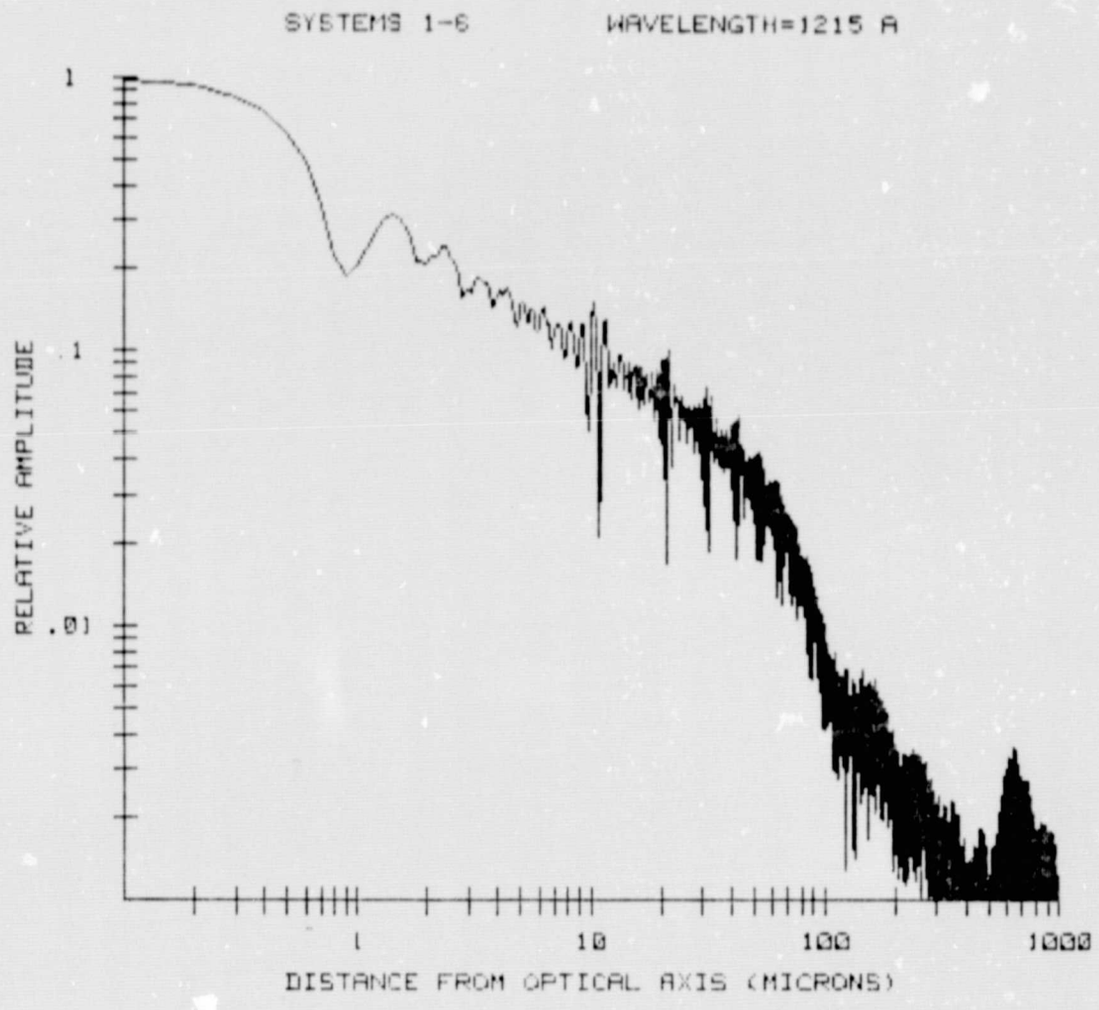

Fig. 40: Diffraction analysis of composite system

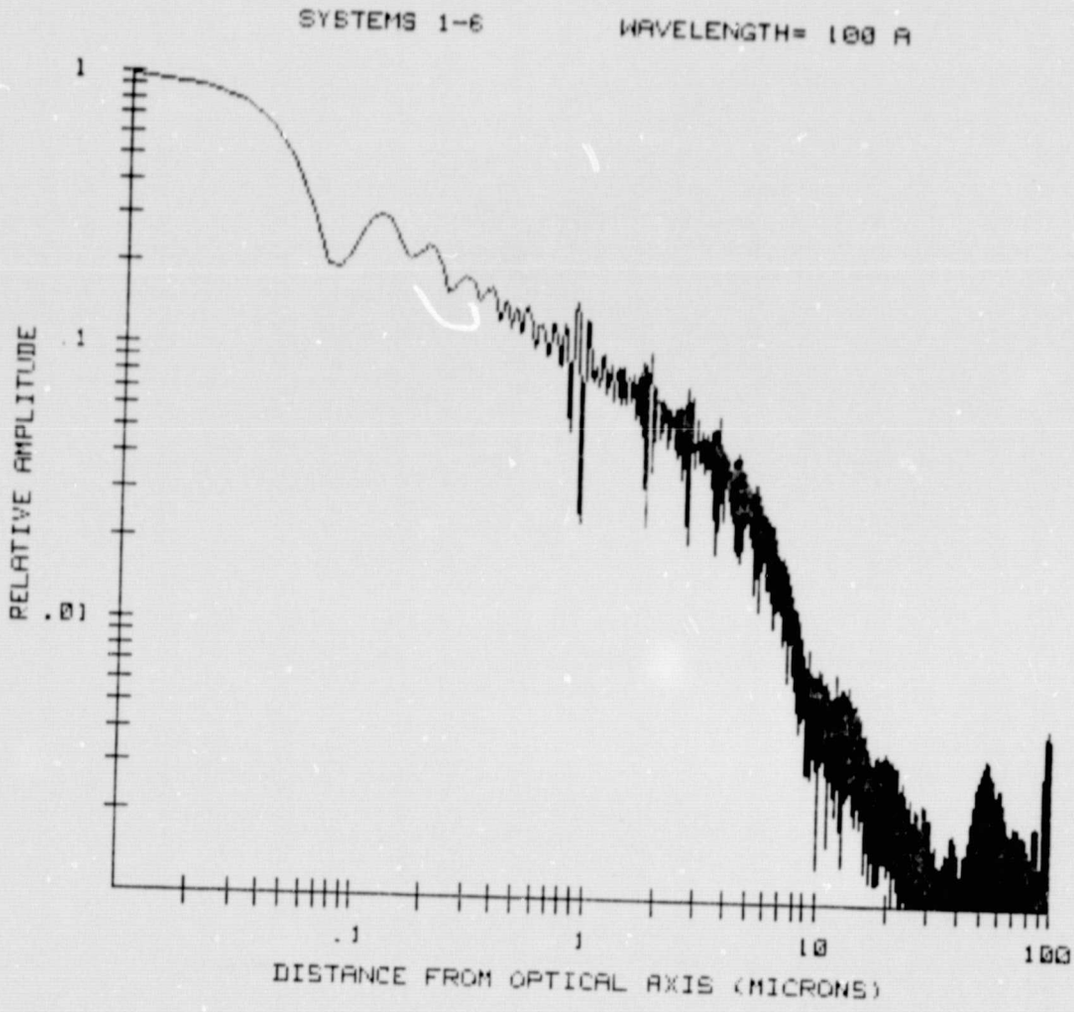

Fig. 41: Diffraction analysis of composite system

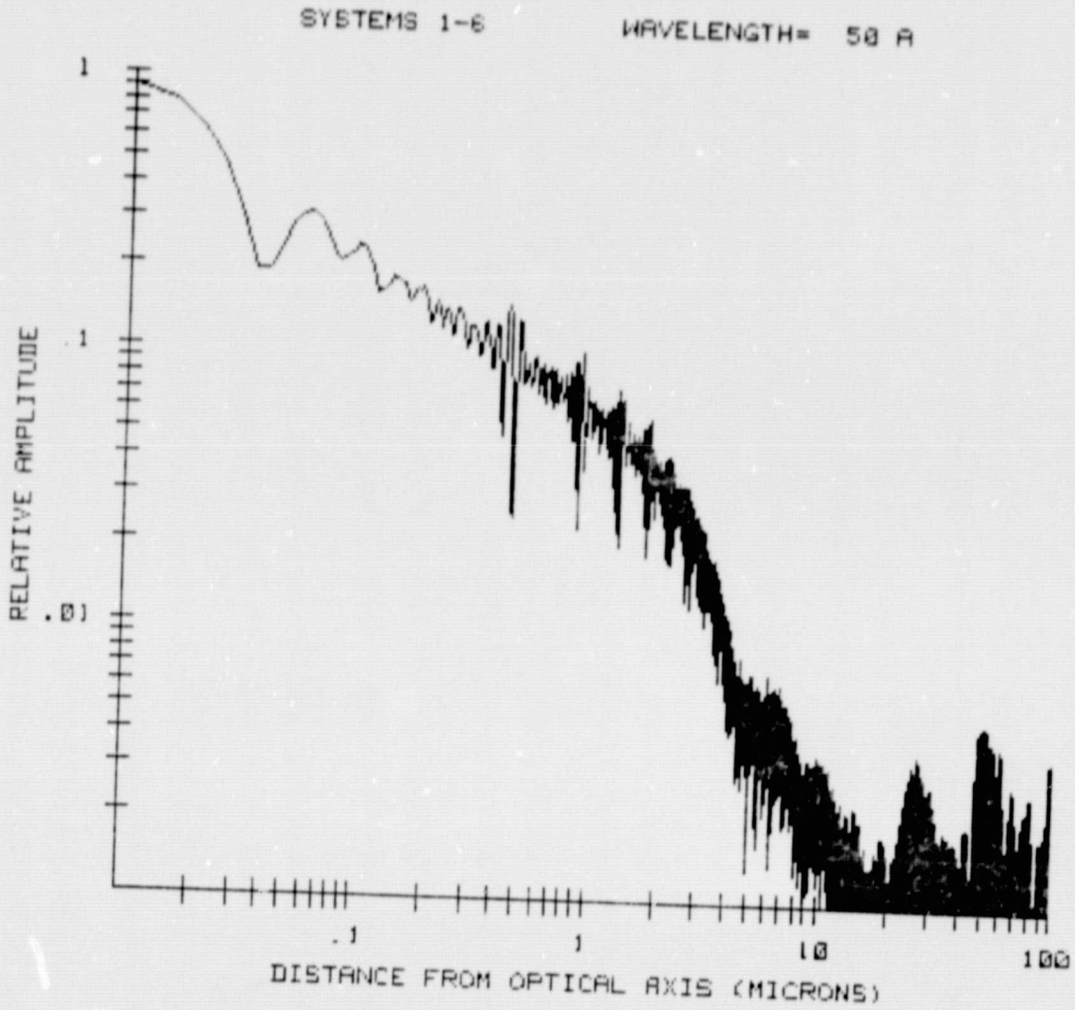

Fig. 42: Diffraction analysis of composite system

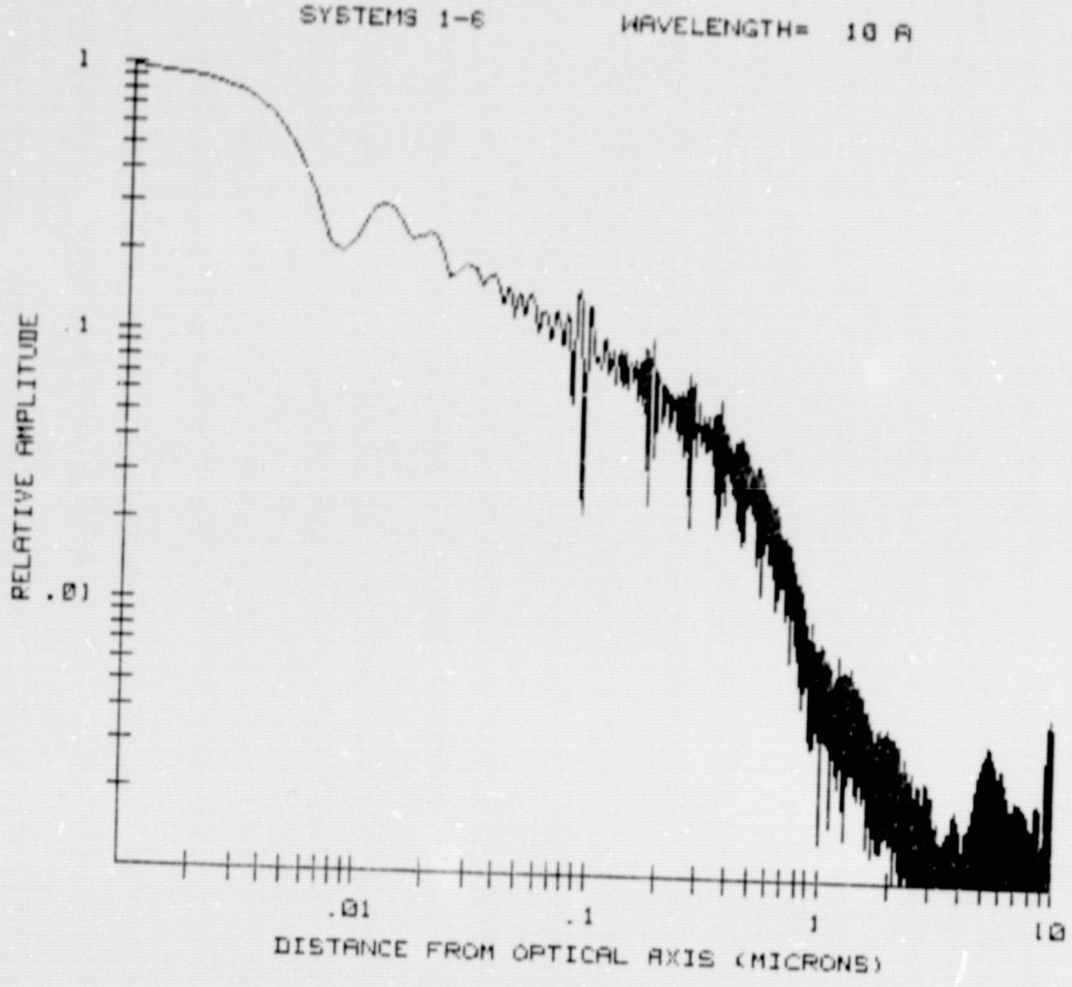

Fig. 43: Diffraction analysis of composite system